

Are granular materials simple? An experimental study of strain gradient effects and localization

Matthew R. Kuhn

*Dept. of Civil and Env. Engrg., Univ. of Portland, 5000 N. Willamette Blvd.,
Portland, OR, U.S.A. 97203*

Tel.: 503-943-7361; Fax: 503-943-7316

Abstract

Experiments test the dependence of shearing stress on the first two gradients of shear strain. The tests were conducted by direct numerical simulation using the Discrete Element Method (DEM) on a large two-dimensional (2D) assembly of circular disks. The assembly was coerced into non-uniformly deformed shapes by applying body forces to the material region. The tests show that shearing stress is affected by both the first and second gradients of shear strain, and the measured responses to strain and its gradients are all incrementally nonlinear. The dilation rate is unaffected by strain gradients. Particle rotations, although highly erratic, are, on average, consistent with the mean-field rotation and unaffected by strain gradients. In independent unconstrained tests, the material was sheared without body forces so that localization could freely occur. Three localization patterns were observed: microbands at very small strains; non-persistent shear bands at moderate strains; and persistent bands at large strains. The observed features of microbands and shear bands are consistent with the measured influences of shearing strain and its first two derivatives.

Key words: Granular material; Microstructures; Localized deformation; Shear bands; Inhomogeneous material Discrete element method

1 Introduction

Noll (1958) defined a simple material as one in which the stress at a material point depends upon the first deformation gradient and its history at that point. The sole dependence upon local strain as the kinematic variable distinguishes simple materials from other, more generalized descriptions, such as those in micro-polar, non-local, and strain gradient models. This paper describes experiments that directly demonstrate that granular materials are non-simple and that shearing stress depends upon the first three gradients of shearing displacement (i.e., the shearing strain and its first two gradients). The experiments were conducted by coercing non-uniform deformations and measuring the local

Email address: kuhn@up.edu (Matthew R. Kuhn).

material response. In the paper, we also address the manner in which shearing deformation can freely localize within a granular material and the relationship between strain gradients and the localization patterns.

Strain gradient effects have been postulated for granular materials, and many gradient-dependent constitutive formulations have already been proposed. Such generalized constitutive proposals have certain attractive features: strain gradient models can be used to construct continuum descriptions of materials that are, in fact, discrete at a micro-scale; non-simple continuum descriptions introduce a characteristic length that can be used to describe scale-dependent localization phenomena; and including higher order deformation gradients within a constitutive framework can circumvent problems of ill-posedness in the associated boundary value problems. Although gradient-dependent models offer these features, there has been no direct experimental evidence that granular materials exhibit such behavior. Indirect experimental evidence has been provided with other materials, such as micro-indentation testing and thin-wire torsional testing (e.g., Fleck and Hutchinson 1997). With granular materials, however, we have the ability—perhaps unique among materials—to observe, measure, and, hopefully, resolve this complexity with numerical experiments that realistically simulate the underlying micro-scale mechanics. The primary means of performing these experiments is the Discrete Element Method (DEM), which has become an effective tool for directly simulating and exploring the mechanical behavior of granular materials at both the particle and macro levels (Cundall and Strack 1979).

The experiments in this paper reveal quite unusual and complex behavior, behavior that has not yet been entirely captured in any continuum description. In one set of experiments, we observe the localization patterns that spontaneously appear during shearing. In other experiments, the effects of the first and second strain gradients are measured by coercing a large assembly of particles into predetermined shapes. The coerced shapes were achieved by applying body forces in a controlled manner. The material response was computed with averaging techniques that allow us to characterize both the average response and the variability of the response under conditions of non-uniform deformation. The paper proceeds as follows:

- Section 2 describes the granular assembly and summarizes the experimental methods.
- Sections 3–5 give the experimental results. Section 3 catalogs the localization patterns that spontaneously appear during unconstrained shearing. Sections 4 and 5 report the cumulative and incremental gradient-dependent responses that were measured in constrained non-uniform shearing.
- In Section 6 we consider some characteristics of the localization patterns that are reported in Section 3 and whether these characteristics are consistent with the gradient-dependent behavior that is reported in Sections 4 and 5.
- Section 7 summarizes the experimental findings.

2 Methods

The work is primarily experimental. Quasi-static numerical simulations were performed on a large rectangular two-dimensional assembly of 10,020 densely packed circular disks (Fig. 1a). Two independent sets of shearing experiments were conducted. The first set was conducted under *unconstrained* conditions in which localization could spontaneously occur. These are the Series I tests described in Sections 2.6 and 3.1. The second set of experiments was conducted under *constrained* conditions that permit the direct

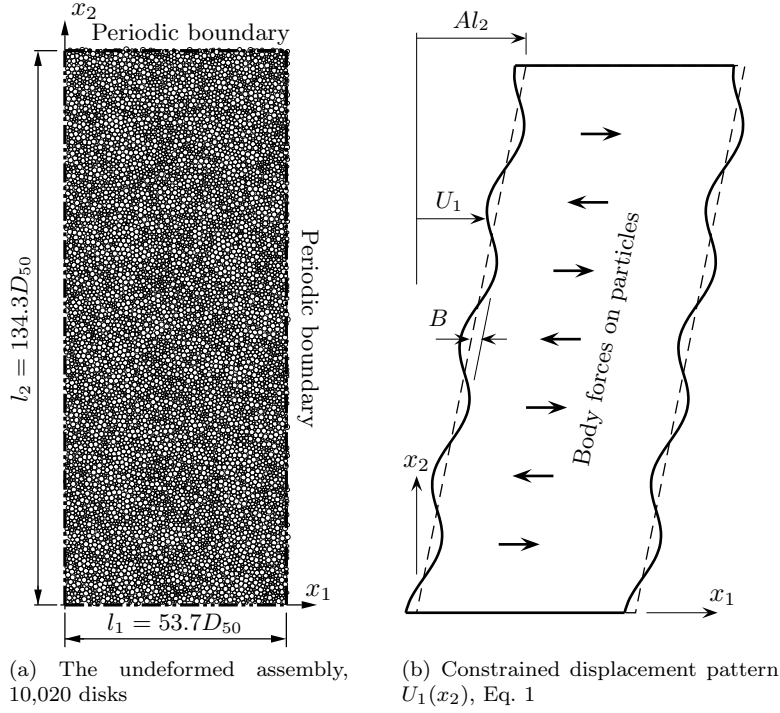


Fig. 1. The assembly of 10,020 disks and a coerced horizontal displacement profile, as in the Series II–IV constrained shear tests.

measurement of strain gradient effects. These are the Series II–IV tests of Sections 2.7–2.9 and 3.2–5.2.

2.1 Description of the material

The assembly height l_2 was about 134 particle diameters and about 2.50 times its width l_1 (Fig. 1a). The particle assembly was surrounded on all sides by periodic boundaries. The diameters of the 10,200 circular disks were randomly distributed within a fairly narrow range of 0.45–1.40 times the median particle diameter D_{50} . The particles were initially assembled and compacted into an irregular but macroscopically isotropic arrangement. The initial assembly was fairly dense, with a void ratio of 0.172 and an average coordination number of 4.04. The contact indentations were small — on average, about 0.11% of D_{50} .

A simple force mechanism was employed at the particle contacts. Linear normal and tangential contact springs were assigned equal stiffnesses, and the coefficient of contact friction was 0.50. Unlike the model of Iwashita and Oda (1998), no rolling resistance was included in the contact mechanism.

2.2 Constraining the deformations

Both constrained and unconstrained shearing tests were conducted. To study the effects of strain gradients, non-uniform shearing deformations were coerced in a controlled manner by applying horizontal body forces to particles throughout the assembly. The numerical algorithm, a modification of the Discrete Element Method (DEM), produces a progressively more deformed sinusoid shape (Fig. 1b). Individual particles, however, were allowed to freely move and rotate within their neighborhoods of particles, provided that,

on average, the particles moved in collective accord with the prescribed sinusoid contour. The numerical algorithms are described elsewhere (Kuhn 2003).

In tests with constrained deformations, the assembly was slowly and progressively sheared through a sequence of horizontal displaced shapes U_1 (Fig. 1b),

$$U_1(x_2, t) = A(t)x_2 + B(t) \cos \left(\frac{2\pi n}{l_2} x_2 - \phi \right) \quad (1)$$

which were predetermined by the controlling shape parameters $A(t)$, $B(t)$, n , and ϕ . The horizontal shearing strain γ and its first two gradients, γ' and γ'' , are directly computed as

$$\gamma(x_2, t) \equiv \partial U_1 / \partial x_2 \quad (2)$$

$$= A(t) - B(t) \frac{2\pi n}{l_2} \sin \left(\frac{2\pi n}{l_2} x_2 - \phi \right)$$

$$\gamma'(x_2, t) \equiv \partial^2 U_1 / \partial x_2^2 \quad (3)$$

$$= -B(t) \left(\frac{2\pi n}{l_2} \right)^2 \cos \left(\frac{2\pi n}{l_2} x_2 - \phi \right)$$

$$\gamma''(x_2, t) \equiv \partial^3 U_1 / \partial x_2^3 \quad (4)$$

$$= B(t) \left(\frac{2\pi n}{l_2} \right)^3 \sin \left(\frac{2\pi n}{l_2} x_2 - \phi \right).$$

In each simulation experiment, the values of n and ϕ were held constant, while A and B were advanced in small steps. The separate effects of γ , γ' , and γ'' were investigated by running numerous simulations with different n and ϕ values and by slowly advancing the progressions of $A(t)$ and $B(t)$ (Sections 2.7–2.9).

The assembly width l_1 was maintained constant during all simulations, but vertical dilation was freely allowed under the condition of a constant vertical stress $\bar{\sigma}_{22}$ (Section 4.4). The horizontal displacement U_1 in equation (1) represents a circumstance that was only satisfied *in the mean* by the 10,020 particles. The movement of each, k^{th} individual particle, u_1^k , was free to fluctuate about the mean U_1 , as is shown in Fig. 2. The particle movements in the figure are measured relative to their positions in the undeformed assembly (at strain $\gamma = 0$) and have been normalized by dividing by the median particle diameter D_{50} , which we adopt as the fundamental unit of length.

2.3 Body forces and stress

The constrained displacement contours (1) were produced by applying a horizontal body force to each particle in the assembly Kuhn (2003). The algorithm produces an erratic distribution of body forces b_1^k , as is apparent in the scatter plot of Fig. 3a. We are primarily interested in the horizontal shearing stress $\bar{\sigma}_{21}$ and its variation along the height of the assembly. Because stress is highly non-uniform within granular materials, averaging techniques were required to arrive at a representative shearing stress at any vertical level x_2 within the assembly. The horizontal shearing stress $\bar{\sigma}_{21}$ across a level x_2 was computed in the manner suggested by Bagi (1999). This shearing stress is an average *local* stress, computed across surfaces (or within thin horizontal regions) that encompass about 80 particles, which could be considered the size of the representative volume element (RVE) of this study. The shear stress within such small regions will likely vary greatly

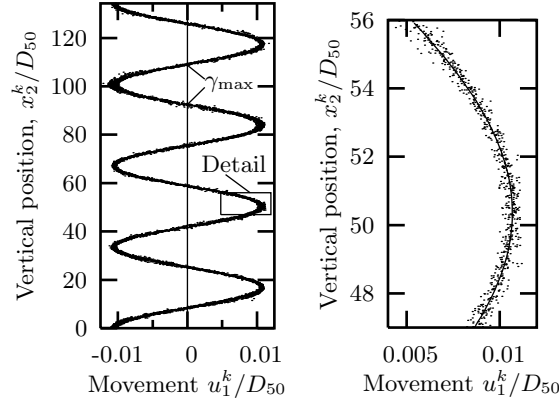


Fig. 2. Horizontal movements of the 10,020 particles in a single Series III sinusoid shear test (Eq. 1: $n = 4$, $\phi = 0$, $A = 0$, $B = -0.011D_{50}$) Each dot represents the displaced center of a single (k^{th}) particle.

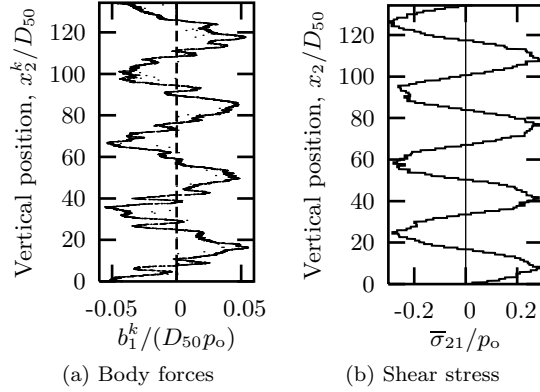


Fig. 3. Horizontal body forces and shear stress within the assembly for the displacement profile shown in Fig. 2.

within the assembly, and this variability is the topic of Section 4.6. The rather substantial variability was partially moderated, however, with averaging techniques that are described in Section 2.8.

2.4 Phase-space representations

A phase-space can be used to represent combinations of shearing deformation γ and its gradients γ' and γ'' , with each point in the phase-space representing a possible deformation condition within a small material region. The independent variable is the vertical position x_2 rather than time, as would be the case in the usual phase-space representations of oscillatory phenomena. In a phase-plane of $\gamma - \gamma'$ (as in Fig. 4), uniform shear is simply a single point on the γ axis; a strain discontinuity is represented by two separated points; and a smooth shear band is represented by a loop or, perhaps, by a broken loop. In the absence of horizontal body forces, these phase trajectories represent the locus of combinations γ , γ' , and γ'' that would produce the same shearing stress σ_{21} on horizontal planes. We are particularly interested in the possible presence of loop trajectories within a family (phase portrait) of constant-stress trajectories, as such loops indicate that the material could

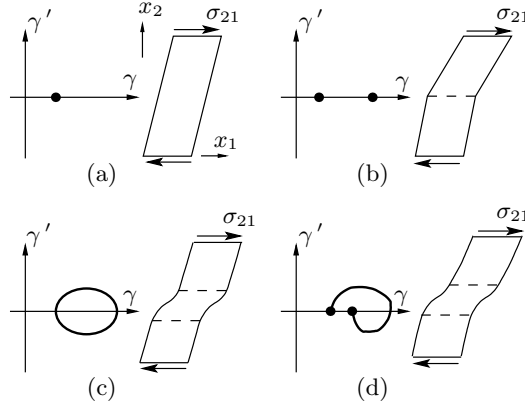


Fig. 4. Phase-plane representations of shearing patterns.

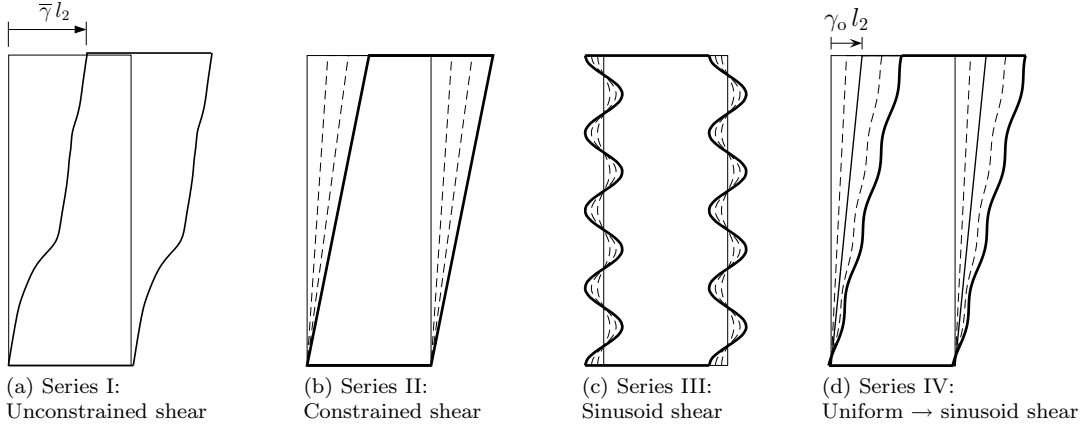


Fig. 5. Horizontal displacement contours in the four series of tests. In Series II–IV, the deformations were coerced (constrained) by the application of body forces.

support a shear band. Our experiments allow the mapping of large portions of the phase portrait for the assembly of 10,020 particles, as will be seen in later sections.

2.5 Testing series

Four series of tests were performed on the particle assembly, either by permitting unconstrained deformation or by coercing the assembly through prescribed sequences of predetermined shapes (Fig. 5). These tests can be separated into two types having different purposes:

- Series I tests were conducted under *unconstrained* conditions without body forces, so that localization patterns were free to spontaneously develop (Fig. 5a). These patterns were observed and cataloged.
- Series II, III, and IV tests were conducted under coerced, *constrained* conditions that disallowed shearing localization (Figs. 5b–d). Body forces were applied to attain predetermined sequences of shapes, with the intent of observing and measuring the effects of strain gradients on the shearing response.

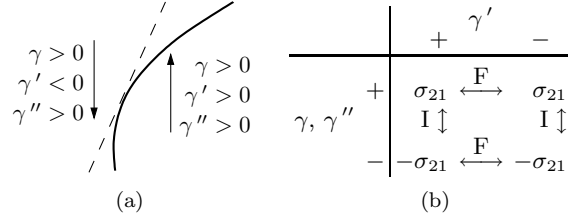


Fig. 6. Material frame indifference and isotropy for a one-dimensional continuum. The relations “I” and “F” are consequences of isotropy and objectivity, respectively.

2.6 Series I tests: Unconstrained shear

In Series I tests, the shearing was produced by slowly moving the upper boundary horizontally at a rate $\dot{\gamma}l_2$ relative to the lower boundary (Fig. 5a). Unlike the other series of tests, no predetermined shape was imposed upon the assembly, so that shear bands and other localization patterns could freely develop within the assembly. Furthermore, no body forces were applied to the particles, so that the horizontal shearing stress $\bar{\sigma}_{21}$ was uniform throughout the height of the assembly.

2.7 Series II tests: Constrained uniform shear

This series of tests coerced a *uniform shearing profile* along the entire height of the assembly, l_2 , with the sinusoid parameter B set to zero (Eq. 1 and Fig. 5b). Unlike the unconstrained Series I tests, a uniformly deformed shape was attained by applying body forces, which disallowed the formation of shear bands within the assembly and minimized the strain gradients γ' and γ'' .

2.8 Series III tests: Monotonic sinusoid shear

In the Series III tests, the deformation profile was entirely sinusoid, with the shape parameter A set to zero (Eq. 1 and Fig. 5c). The Series III tests intentionally produced non-uniform deformations, with non-zero shearing gradients γ' and γ'' along the height of the assembly. This series included 50 tests having various combinations of the shape parameters n and ϕ , so that the separate effects of γ' and γ'' could be distinguished (Eq. 1). The integer n ranged from 1 to 8, with larger values producing deformations having greater strain gradients. The largest value of $n = 8$ produced 16 half-sinusoid deformation zones, which might be likened to half-sinusoid shear bands of width $l_2/16$, or about $8.4D_{50}$ —somewhat thinner than typical shear band widths. Tests conducted with the same n but with different phase angles ϕ simply shifted the deformation pattern so that 64 to 128 samples of the stress-strain behavior could be captured and averaged along the height of the assembly.

In the Series III tests, the shear strain and its gradients were advanced in a monotonic and proportional manner, so that the ratios γ'/γ and γ''/γ remained constant at any level x_2 within the assembly. By taking advantage of material frame indifference (objectivity) and isotropy, the behaviors at several levels x_2 can be folded into a single quadrant of the $\gamma - \gamma' - \gamma''$ phase-space. We note that two observers, each rotated by 180° with respect to the other, would report the same shearing deformation γ , the same second strain gradient γ'' , and the same shearing stress σ_{21} for a given deformation pattern (Fig. 6a). They would, however, report opposite values of the first gradient γ' . A one-dimensional constitutive

Table 1

Increments of $d\gamma$, $d\gamma'$, and $d\gamma''$ applied in Series IV tests after an initial phase of uniform deformation.

Condition	$d\gamma$	$ d\gamma' $	$d\gamma''$
1	+ or -	0	0
2	0	+	0
3	0	0	+ or -
4	+	+	0
5	-	+	0

form for the shearing stress must, therefore, satisfy the condition

$$\sigma_{21}(\gamma, \gamma', \gamma'') = \sigma_{21}(\gamma, -\gamma', \gamma'') , \quad (5)$$

which implies an intrinsic nonlinearity in γ' . When present in a constitutive form, the gradient γ' should appear, therefore, as a norm, and, henceforth, the gradient γ' will often be written as the magnitude $|\gamma'|$. If the material is isotropic, the shearing stress must also change signs with a change in the signs of both γ and γ'' :

$$\sigma_{21}(\gamma, \gamma', \gamma'') = -\sigma_{21}(-\gamma, \gamma', -\gamma'') . \quad (6)$$

These relationships are summarized in Fig. 6b.

2.9 Series IV tests: Constrained incremental sinusoid shear

A fourth series of tests measured the incremental response to loading and unloading in the presence of strain gradients. These tests allow us to study spontaneous localization after a sustained period of uniform deformation. The assembly was uniformly deformed to predetermined shear strains γ_0 (as in the Series II tests), and then it was deformed in small increments of non-uniform, constrained sinusoid shearing (Fig. 5d). By applying particular combinations of increments dA and dB in Eqs. (1)–(4), one of either $d\gamma$, $|d\gamma'|$, or $d\gamma''$ could be advanced, while the other two would remain stationary (Table 1). These combinations were also employed to reconcile possible incremental nonlinearities associated with loading or unloading. In addition to probing the separate incremental effects of $d\gamma$, $|d\gamma'|$, and $d\gamma''$, two other sets of tests were conducted to investigate the possible coupling of the incremental effects of strain $d\gamma$ and its first gradient $|d\gamma'|$ (Table 1, Conditions 4 and 5).

3 Results: localization and uniform shearing (Series I and II tests)

3.1 Localization patterns (Series I tests)

Localization was explored with a Series I test, which produced shearing along the height of the assembly, but under unconstrained conditions that allowed spontaneous localization (Section 2.6 and Fig. 5a). Three localization patterns were observed: thin microbands at small strains, non-persistent shear bands at moderate strains, and a solitary persistent shear band just prior to and following the onset of strain softening.

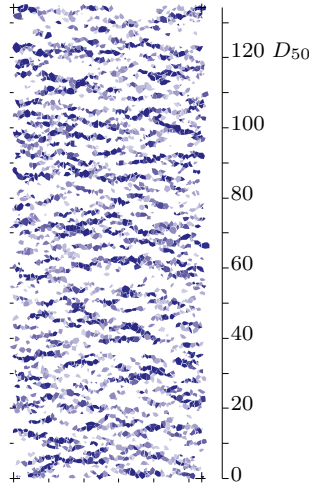


Fig. 7. Microband deformation patterns at small strains in a Series I test ($\gamma = 0.01\%$).

3.1.1 Microbands at small strains

Microbands, thin zones of intense shearing, can appear at low strains, and even at the very start of shear loading (Kuhn 1999). Figure 7 shows the local shearing deformations at the start of a Series I unconstrained shear test. The figure displays the horizontal shearing rates within the smallest possible regions for which a deformation measurement would be meaningful—the small polygonal void cells within circuits of adjacent particles (see Kuhn 1999). Figure 7 reveals a network of microbands. Unlike the much thicker shear bands that appear at larger strains, microbands can be as short as $8D_{50}$, with thicknesses of $1\frac{1}{2}$ – $2\frac{1}{2}D_{50}$. The patterning is quite irregular, but the center-to-center spacing between microbands is $3\frac{1}{2}$ – $8D_{50}$. In Section 6.1, we relate this periodicity to the measured dependence of shearing stress on the gradients of strain.

3.1.2 Non-persistent and persistent shear bands at larger strains

Although the horizontal shearing stress was uniform along the assembly’s height l_2 , the shearing deformation was hardly uniform, as is apparent in Fig. 8, which shows the horizontal displacements u_1^k of 10,020 particles at their heights x_2^k within the assembly. In the figure, the shearing strain $\bar{\gamma}$ is 2.5%, and the particle displacements are measured relative to their initial positions at $\gamma = 0$. Both the displacements u_1^k and positions x_2^k are expressed in a dimensionless form by dividing by the median particle diameter D_{50} .

The residual evidence of three deformation bands is apparent in Fig. 8a. Two of the bands, labeled A and B, were not persistent and were no longer active at the 2.5% strain; whereas, band C had just become the sole and persistent shear band. The non-persistent bands A and B were present in varying intensities at shear strains $\bar{\gamma}$ of 0.5–2.1% respectively, and each was, at times, the dominant deformation region. At other times, each band was entirely inactive. Such non-persistent bands have also been observed in biaxial tests on loose sands (Finno et al. 1997). Band C first appeared at a strain of 1.4% but was, at later times, altogether inactive. It became the dominant and persistent band at a strain of 1.85%, shortly before the onset of softening. During the subsequent shearing, the assembly’s deformation was localized entirely within this single zone.

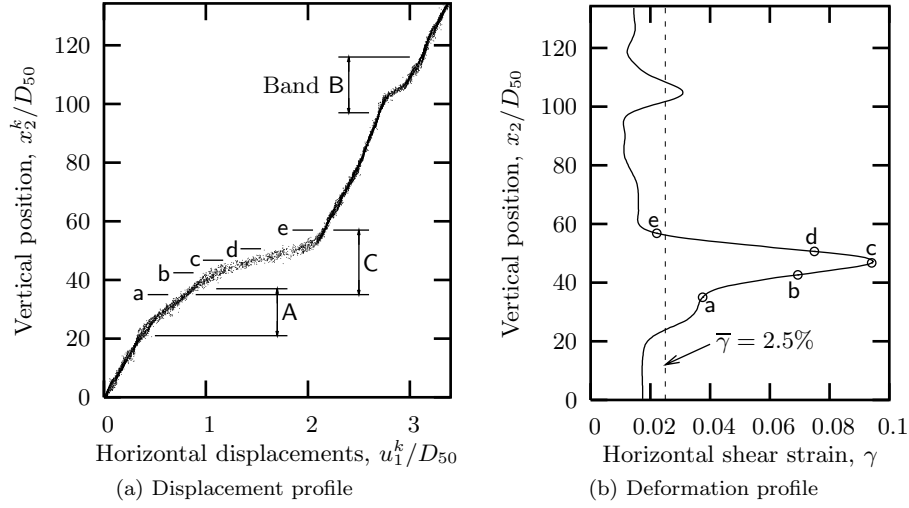


Fig. 8. Results of a Series I test of unconstrained shear for $\bar{\gamma} = 0$ to 2.5%. Three shear bands (labeled A, B, C) appeared at various stages of deformation (see also Fig. 10). Only band C was eventually persistent.

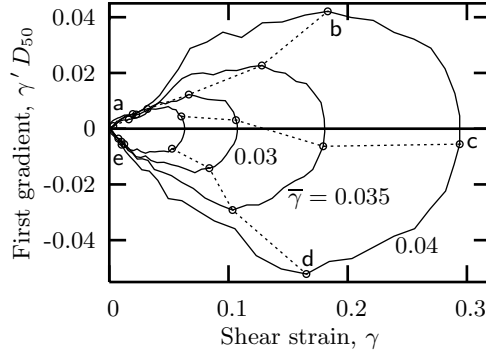


Fig. 9. Phase-plane representation of shear band C during a Series I unconstrained shear test. Points a–e are shown in Fig. 8. Strains and strain gradients are relative to those at $\gamma = 0$.

In these experiments, we see the truly complex influence of heterogeneity on shear band formation, where a local weakness can precipitate a shear band but later heal, while yet other shear bands are forming elsewhere within the material. This transient behavior is also addressed in Sections 4.6 and 6.2.2.

The accumulated strains within the three bands are clearly present in the shear strain profile of Fig. 8b, which gives shearing strains relative to the initial, undeformed assembly. The persistent band C has a thickness of about $20D_{50}$, somewhat greater than that measured in other experiments (see Vardoulakis 1998 for a review).

The deformations can also be represented in the phase-plane of γ and γ' (Fig. 9). The loops in the figure are of band C, which we have highlighted by plotting the conditions at strain intervals of 0.5% relative to the reference strain of $\bar{\gamma} = 2.0\%$. The results show a progressive intensification of local shearing deformation within the band, as is indicated

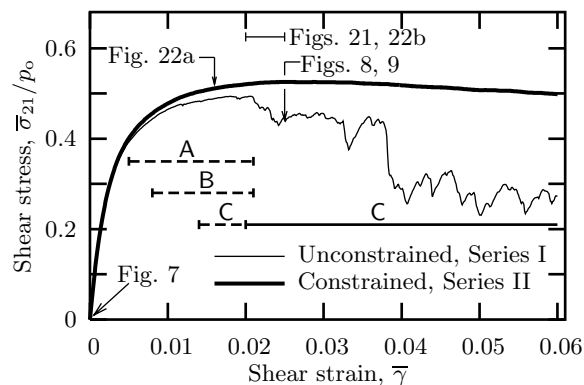


Fig. 10. Comparison of constrained and unconstrained shearing tests (Series I and II, Figs. 5a–b). The three shear bands A, B, and C are shown in Fig. 8.

by the increasing size of the loop trajectories. In this figure, the left ends of the loops cross the vertical γ' -axis, although only slightly. These negative strains indicate a small unloading of the material outside of the shear band C. In Section 6.2 we again consider a phase-space representation of band C, by referencing a simple one-dimensional gradient-dependent model.

3.2 Comparison of constrained and unconstrained shearing (Series I and II)

Shearing stresses for both constrained and unconstrained conditions are compared in Fig. 10. During a constrained Series II test, uniform shearing was coerced along the height of the assembly, using body forces to preclude the appearance of shear bands and microbands (Section 2.7 and Fig. 5b). A constrained test can be thought to measure the average material response, since a gross deformation field was imposed upon the material, disallowing any spontaneous localization within weaker regions. The stresses at low strains are about equal for unconstrained and constrained conditions, but the stresses begin to differ at a strain of about 0.4%, which roughly coincides with the first observation of a non-persistent shear band (band A, Fig. 8). The strengths in Fig. 10 abruptly diverge at a strain of 2.1%, which roughly coincides with the final emergence of band C as the solitary persistent shear band. The rather erratic strength at strains greater than 3.0% is likely due to discrete deformation events that involve, perhaps, a few particles becoming either dislodged or jammed among neighboring particles. Shear band C encompasses fewer than 1500 particles, and such discrete deformation events would likely have a dominant influence among particles that are moving from one meta-stable configuration to another.

4 Results: strain gradient effects for constrained proportional sinusoid shearing (Series III tests)

We now consider the results of Series III tests in which the assembly was progressively coerced into a sinusoid shape (Section 2.8 and Fig. 5c). These tests will directly resolve whether the material is simple or non-simple by scrutinizing the influence of the two gradients of shear strain, γ' and γ'' , under conditions in which γ , γ' , and γ'' were proportionally and monotonically advanced. The incremental response is probed with Series IV tests (Section 5).

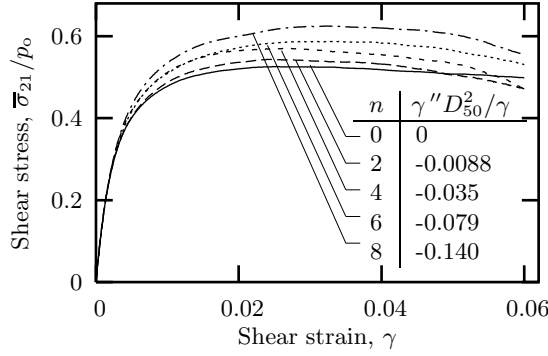


Fig. 11. The measured effect of the second gradient of shearing strain, γ'' , on the stress response of the material.

4.1 Effect of second gradient γ'' at large strains

The effect of the second gradient γ'' can be isolated by comparing tests with different values of the shape parameter n (see Eqs. 1–4). Larger n values displace the assembly into sinusoid profiles having more tightly spaced cycles with larger gradients γ'' . Although both γ and γ'' increase as the assembly is progressively deformed, the dimensionless ratio $\gamma'' D_{50}^2/\gamma$ remains constant throughout the assembly and depends only upon the value of n :

$$\frac{\gamma'' D_{50}^2}{\gamma} = - \left(\frac{2\pi n}{l_2/D_{50}} \right)^2 \quad (7)$$

as in Eqs. 2 and 4 with $A = 0$. With values of n ranging from 1 to 8, we can explore the material's response to a range of negative ratios $\gamma'' D_{50}^2/\gamma$, from nearly zero to about -0.140 . This range of ratios fully encompasses the *negative* gradients γ'' that would be expected near the center of a shear band. We should note, however, that in these Series III tests, the ratio (7) is always negative, so that the tests could not explore the effects of positive ratios γ''/γ , which will occur along the outer portions of a shear band (Section 6.2.1).

The measured effect of the second gradient γ'' is shown in Fig. 11. The shearing stress $\bar{\sigma}_{21}/p_o$ and the shearing strain γ are plotted for various ratios of $\gamma'' D_{50}^2/\gamma$ (Eq. 7). Each line is an average of as many as 128 samples that were subjected to the same deformation sequence. The single solid line for ratio $\gamma'' D_{50}^2/\gamma = 0$ is borrowed from the Series II tests in which the assembly was uniformly sheared under constrained conditions (Sections 2.7 and 3.2). For a classical, simple continuum, the stress-strain response is independent of γ'' . The data shows, however, that a negative second gradient γ'' has a moderate hardening effect on granular materials, increasing the local yield strength. Figure 11 shows the averaged results for all locations x_2 at which the first gradient γ' was equal to zero, so that the effect of the second gradient γ'' is entirely isolated. This particular condition of a negative second gradient γ'' and a first gradient $\gamma' = 0$ would be expected to occur at the mid-thickness of a developing shear band (at point “c” in the shear band C of Figs. 8 and 9). Increasingly negative values of the ratio $\gamma'' D_{50}^2/\gamma$ produce a larger hardening effect, although even with low ratios, the hardening effect is still active. The smaller ratios correspond to half-sine thicknesses of 30 or more particle diameters, indicating that the hardening effect of the second gradient γ'' may be active

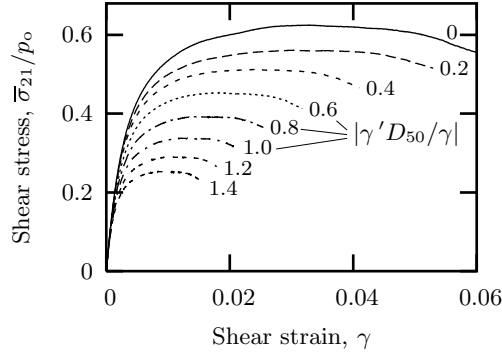


Fig. 12. The measured effect of the first gradient of shear strain, γ' , on the stress response of the granular material.

across quite large distances. The lines in Fig. 11 appear to merge at small strains, but subtle differences are present in the initial slopes, and these differences can be attributed to the second gradient γ'' , a phenomenon that is viewed more closely in Sections 5.1 and 6.1.

4.2 Effect of first gradient γ' at large strains

The Series III tests also resolved the separate effect of the first gradient of shear strain. A strong softening effect of the gradient γ' is revealed by comparing the material's response at different locations x_2 within the assembly. Equations (2) and (3) can be arranged into an expression for the first strain gradient,

$$\frac{\gamma' D_{50}}{\gamma} = \frac{2\pi n}{l_2/D_{50}} \cot \left(\frac{2\pi n}{l_2} x_2 - \phi \right), \quad (8)$$

noting that shape parameter $A = 0$ in the Series III tests. For a test in which the parameters n and ϕ have been prescribed, the dimensionless ratio $\gamma' D_{50}/\gamma$ depends only on the position x_2 . Because of spatial symmetries in the sinusoid displacement profile, the averaged results can be presented in the form of the positive ratio $|\gamma' D_{50}/\gamma|$ (Section 2.8).

Figure 12 shows the averaged stress response at various ratios $|\gamma' D_{50}/\gamma|$ for tests in which $n = 8$. Each line shows the response to a different ratio $|\gamma' D_{50}/\gamma|$ and is the averaged behavior of as many as 128 material samples. The figure documents a rather substantial softening effect of the first gradient γ' under monotonic loading conditions in which γ , γ' , and γ'' progress in a proportional manner.

In the previous section, a negative second gradient γ'' was shown to have a moderate hardening influence on granular materials. This influence was apparent in Fig. 11 for conditions with $\gamma' = 0$. At even moderate ratios $|\gamma' D_{50}/\gamma|$ of 0.4 or greater, the hardening effect of a negative γ'' is, however, entirely counteracted by the softening influence of the first gradient γ' .

The contour plot of Fig. 13 shows the combined effects of both the shear strain γ and its dimensionless gradient $|\gamma' D_{50}|$ upon the shear stress $\bar{\sigma}_{21}/p_o$. Because of spatial symmetries in the Series III tests, the full phase-plane can be folded and averaged into a single quadrant (Section 2.8). Figure 13 displays looped contours for stress ratios $\bar{\sigma}_{21}/p_o$ in the range of about 0.55–0.62, which resemble the looped phase trajectories of the shear bands that

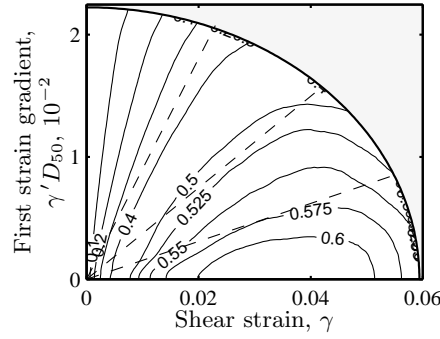


Fig. 13. Contours of the shearing stress $\bar{\sigma}_{21}/p_0$. The results are from tests in which γ and γ' were increased in a proportional manner, as indicated by the dashed radial lines (Series III, $n = 8$, $\gamma'' D_{50}/\gamma = -0.140$).

were depicted in Figs. 4c–d. Although the looped contours in Fig. 13 might support the existence of a shear band, the contours, by themselves, give no indication of how a band could spontaneously form and then intensify. If a region is, at first, deforming uniformly, as would be represented by a single point on the γ axis (Fig. 4a), the phase trajectory must somehow open into a looped trajectory at the start of a band-like localization. (Figs. 4b, c, or d). Such incremental transformations are experimentally investigated with Series IV tests in Sections 5.2 and 6.2.2.

4.3 Constitutive implications

Except in micro-polar formulations, the influence of the first strain gradient is usually excluded in gradient-dependent constitutive proposals. Two rationales have been advanced for negating the influence of the first gradient of strain. One argument arises in efforts to derive the constitutive behavior of a granular material by averaging of the influence of surrounding particles upon a single representative particle (Koenders 1990; Mühlhaus and Oka 1994; Chang and Gao 1995). If the derivation is to be independent of the delegate particle, then the statistical distribution of its neighborhood must exhibit a central symmetry: the particle's neighborhood in a direction \mathbf{n} must be equivalent to that in the opposite direction $-\mathbf{n}$. The combined assumptions of central symmetry and a linear contact behavior cancel the possible effects of the first and all other odd-ordered gradients of strain. A second argument arises when gradient-dependent formulations are derived as approximations of non-local, integral-type constitutive forms (Bažant et al. 1984; Vardoulakis and Aifantis 1991; Vermeer and Brinkgreve 1994). In this approach, the stress at a material point \mathbf{x} is expressed as a functional of the strain in a finite neighborhood \mathcal{B} of the point, usually as an averaged strain $\bar{\epsilon}$. The surrounding deformations are averaged with a weighting kernel Φ ,

$$\bar{\epsilon}(\mathbf{x}) = \int_{\mathcal{B}} \Phi(\mathbf{x} - \mathbf{x}') \epsilon(\mathbf{x}') dV, \quad (9)$$

and the integrand is then approximated with a Taylor polynomial in the strain $\epsilon(\mathbf{x}')$ and its gradients. The combined assumptions of a centrally symmetric kernel, with $\Phi(\mathbf{u}) = \Phi(-\mathbf{u})$, and a symmetric region \mathcal{B} cancel the influence of odd-ordered gradients of strain.

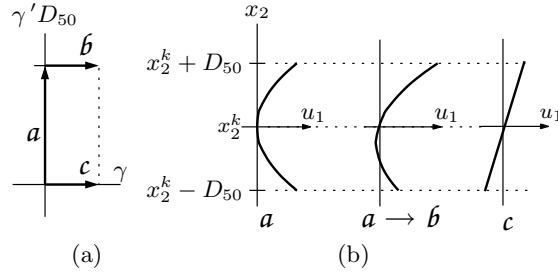


Fig. 14. Different deformation sequences and their relation to a material's central symmetry.

The strong measured influence of the first gradient γ' in the current experiments suggests that central symmetry is invalid when applied to granular materials. Two possible reasons for this invalidation can be surmised by considering a single representative, k^{th} , granule centered at a vertical position x_2^k within the assembly (Fig. 14). We can suppose a non-uniform deformation field in which the entire assembly is deformed by horizontal movements $u_1(x_2)$ that produce no shearing strain γ at the level x_2^k but produce a large gradient of strain γ' . These conditions near x_2^k are represented with path “*a*” in the phase-plane of Fig. 14a. We can also suppose that the reference granule is in contact with several neighboring particles, including particles at $x_2^k + D_{50}$ and $x_2^k - D_{50}$. If the relative movements of the three particles are large, frictional slipping might occur at their contacts. In granular materials, such inelastic response is accompanied by significant changes in the material's fabric (e.g., Oda et al. 1980). Because of the opposite directions of shearing at the two locations, fabric changes will be quite different at $x_2^k + D_{50}$ and $x_2^k - D_{50}$, and any initial central symmetry would be lost. Suppose also that this first stage of deformation is followed by a second stage that produces a small uniform shearing strain γ at level x_2 , as with path “*b*” in Fig. 14a. Due to the nonlinear nature of the contact mechanism, the previous stage *a* of non-uniform deformation will alter the incremental response to the new shearing deformation *b*. The neighboring particle at position $x_2^k + D_{50}$ will likely continue to slip across the reference particle; whereas, slipping would cease with the particle at $x_2^k - D_{50}$, as its contact is unloaded by the *b* displacements. Because of this nonlinearity in the contact mechanism, the central symmetry is further broken by the previous stage *a* of non-uniform deformation. The response through stages *a* and *b* would likely differ, therefore, from that produced by uniform deformation alone (for example, by the path “*c*” in Fig. 14). The experimental results suggest that central symmetry is annulled in a manner that produces substantial gradient-dependent behavior in granular materials.

4.4 Dilatancy

The material in this study dilated as it was sheared—a distinctive characteristic of granular materials. During the constrained uniform shearing of Series II tests, the rate of volume increase was as large as 0.30 times the shearing rate $\dot{\gamma}$. With the sinusoid Series III tests, we can investigate whether the dilation rate depends on either of the two gradients γ' or γ'' under conditions in which γ , γ' , and γ'' advance proportionally.

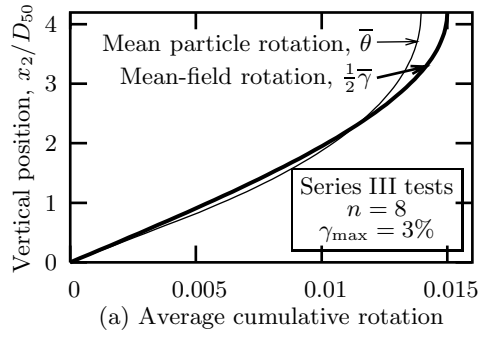


Fig. 15. Comparison of the mean rotations $\bar{\theta}$ of individual particles and the local mean-field rotation $\gamma/2$.

Although dilation does depend upon the shearing strain γ , the tests disclosed minimal dependence of the dilation rate upon either the first or second gradients of shear strain. The dilation that accompanies shearing is generally thought to contribute to the peak strength of granular materials. The current experiments show that the gradients γ' and γ'' can affect the material's strength, but not through any coupling between the dilation rate and the gradients of strain. The results also show that the large dilation within a shear band is caused by the large strains, not by the gradients of strain.

4.5 Particle rotations

In a Cosserat framework of generalized continua, rotations and displacements are treated as independent fields, so that the rotation of a material point can differ from the mean rotation of its neighborhood (i.e. the *mean-field rotation*). However, simulations and physical experiments have shown that although individual particle rotations can differ greatly from the mean rotation field, the mean particle rotation is very close to the mean-field rotation (e.g., Calvetti et al. 1997). The current work provides an opportunity to test whether the *mean rotation field* differs from the *mean-field rotation* under conditions of non-uniform deformation.

The two fields are compared in Fig. 15, using data from four Series III tests with $n = 8$, in which the gradients of strain were quite large. By running multiple tests, the mean rotation field $\bar{\theta}(x_2)$ in Fig. 15 was averaged and smoothed from the rotations of about 40,000 sample particles. The figure shows that the mean rotation field and the mean-field rotation are nearly equal. Any small differences likely result from the averaging of particle rotations that exhibit considerable variation: the standard deviation of particle spins is remarkably about 12 times the mean-field spin. These large variations in particle rotation underscore the difficulty of ascribing continuum behavior to discrete systems of particles.

4.6 Spatial variations in the shearing response

Until now, we have only considered the averaged material response. Localized deformation likely initiates in locally weak regions, as will be demonstrated in Section 6.2.2, and we currently consider the extent of these spatial variations in strength. The responses of 96 samples to the same $\gamma - \gamma' - \gamma''$ loading path are shown in Fig. 16. For each sample, the shear strain and its gradients advanced in a proportional manner, with the ratios $|\gamma'D_{50}/\gamma|$ and $\gamma''D_{50}^2/\gamma$ remaining 0.20 and -0.079 respectively.

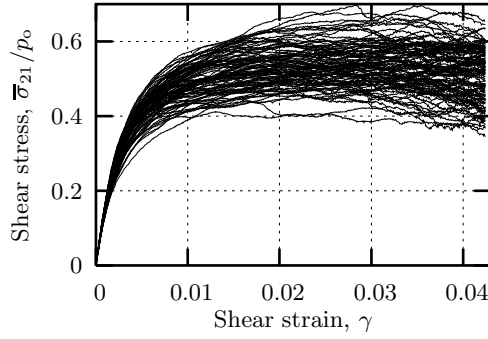


Fig. 16. The spatial variation in strengths among 96 samples in a set of Series III tests.

Figure 16 reveals a rather large variation in the local response among the 96 samples, each containing about 70 particles. In this respect, the local behavior could be more properly referred to as a “range of behaviors.” The range became larger with increasing strain, but was significant even at very low strains.

The many lines in Fig. 16 are highly intertwined, so that the ordering of strengths among the 96 samples was constantly being rearranged. Zones that were weaker at one instant could later heal and strengthen. This lack of temporal coherence can be quantified by comparing the 96 strengths at two different strains, say 1% and 4%, for which the coefficient of correlation was only 0.54.

5 Results: strain gradient effects during incremental sinusoid shear (Series IV tests)

The tests in the previous section were conducted with loading that was monotonic and proportional. In this section, we consider the *incremental behavior* exhibited in Series IV tests, in which a sustained stage of constrained uniform shearing was followed by increments of constrained sinusoid shearing (see Sections 2.9 and Fig. 5d). Such experiments will aid in constructing a gradient-dependent flow theory and in investigating the possible development of localization bands after a sustained period of uniform shearing, as in Section 6.2. We begin by addressing the incremental behavior at the start of loading, and then we consider the incremental response after an extended stage of uniform deformation.

5.1 Incremental effects $|\gamma'|$ and γ'' at small strains

At the start of loading, the first strain gradient γ' had no discernible effect upon the material stiffness. This observation suggests that, on average, the local material behavior exhibits the sort of central symmetry, discussed in Section 4.3, although this symmetry subsequently disappears at larger strains. The central symmetry at small strain is consistent with the conditions that were present in the initial particle configuration: the initial particle arrangement was isotropic, and the particle contact behavior was initially elastic.

At small strains, a negative gradient γ'' *reduces* the material’s initial stiffness. This behavior is opposite that observed at large strains, where an increasingly negative second gradient γ'' was found to have a cumulative hardening effect (Section 4.2). The small strain behavior is detailed in Fig. 17, which shows the initial shear modulus and its dependence on the ratio $\gamma'' D_{50}^2/\gamma$. In the figure, the apparent small-strain shear modulus $G' \equiv \partial \bar{\sigma}_{21}/\partial \gamma$ has been normalized by dividing by the initial pressure $p_o \equiv -\frac{1}{2}\bar{\sigma}_{ii}$. Each of the nine

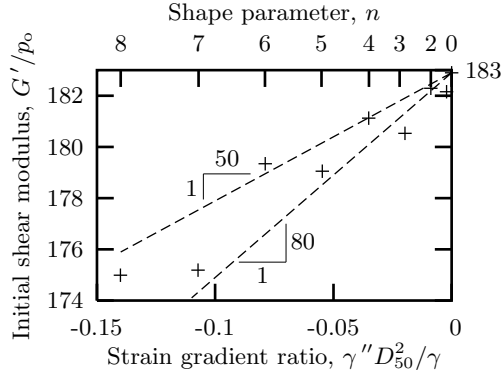


Fig. 17. The effect of the second gradient of shear strain, γ'' , on the initial, small-strain shear modulus G' .

data points corresponds to a single value of the shape parameter n , ranging from 0 to 8 (Eqs. 1–4), and each data point represents the averaged response of as many as 128 material samples. The data was collected in locations x_2 at which the first strain gradient γ' was zero (as in Fig. 11). The results in Fig. 17 are approximated as

$$G' \approx G_o + B_2(\gamma''/\gamma), \quad (10)$$

where B_2 is between $50D_{50}^2p_o$ and $80D_{50}^2p_o$, and the reference shear modulus G_o is about $183p_o$.

5.2 Incremental effects of γ , $|d\gamma'|$, and γ'' at large strains

Series IV tests were used to measure the separate incremental effects of shear strain and its gradients at larger strains (Fig. 5d). The increments $d\gamma$, $|d\gamma'|$, and $d\gamma''$ were applied after an initial stage of steady uniform shearing to seven different predetermined strains γ_o , ranging from 0.5% to 5% (Section 2.9). The tests reveal that the incremental response depends upon each of the increments $d\gamma$, $|d\gamma'|$, and $d\gamma''$. The measured response of the shearing stress $d\bar{\sigma}_{21}$ can be approximated in the following form:

$$d\bar{\sigma}_{21} \approx G^{\text{ep}}d\gamma + B_1^{\text{ep}}|d\gamma'| + B_2^{\text{ep}}d\gamma''. \quad (11)$$

Measured values of the elasto-plastic moduli G^{ep} , B_1^{ep} , and B_2^{ep} are given in Table 2, noting that incremental non-linearities in the first and third terms of (11) are expressed with different loading and unloading stiffness for G^{ep} and B_2^{ep} . The effects of the shearing strain and its first two gradients are shown as being uncoupled in (11). We will soon see, however, that the influences of $d\gamma$ and $|d\gamma'|$ are likely interdependent.

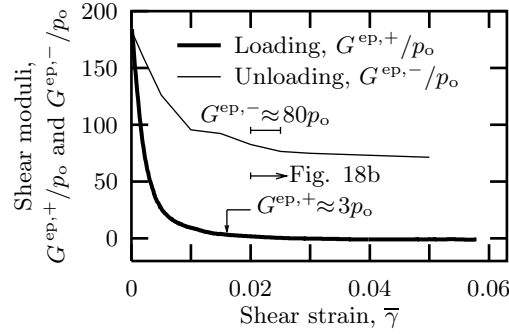
During loading (+), the elasto-plastic shear stiffness $G^{\text{ep},+}$ is simply the slope of the stress-strain curve in Fig. 10, and this slope becomes slightly negative at strains larger than 2.7% (Fig. 18). The *unloading stiffness* $G^{\text{ep},-}$ was continually degraded during the loading process.

A negative second strain gradient $d\gamma''$ has an incremental stiffening effect on the material, with an associated negative modulus B_2^{ep} . Although this influence is consistent with the cumulative effect of γ'' during proportional loading (Section 4.1), it is opposite

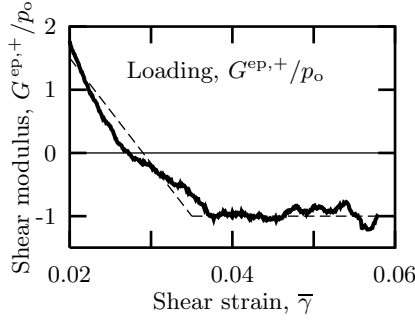
Table 2

Experimentally measured incremental stiffnesses for Eq. 11.

Stiffness	Conditions	Values ^a
$G^{\text{ep},+}$	Loading, $d\gamma/\gamma_o > 0$	Fig. 18
$G^{\text{ep},-}$	Unloading, $d\gamma/\gamma_o < 0$	Fig. 18
B_1	$d\gamma = 0$	$-14D_{50}p_o$
	$ d\gamma' D_{50}/d\gamma = -0.4$	$-11D_{50}p_o$
	$ d\gamma' D_{50}/d\gamma = 0.4$	$-3D_{50}p_o$
$B_2^{\text{ep},+}$	$d\gamma''/\gamma_o > 0, d\gamma = 0$	$-100D_{50}^2p_o$
$B_2^{\text{ep},-}$	$d\gamma''/\gamma_o < 0, d\gamma = 0$	$-16D_{50}^2p_o$
^a also see Fig. 20 for values of B_1^{ep}		



(a) Loading and unloading moduli



(b) Detail of loading moduli

Fig. 18. The incremental shear moduli, for both loading and unloading, as a function of the advancing shear strain.

the incremental effect at small strain, where B_2 is positive (Sections 4.1 and 5.1). The incremental stiffness B_2^{ep} is discontinuous: the value of B_2^{ep} is more negative when $d\gamma''$ is in the same direction as the cumulative shear strain γ_o ($d\gamma''/\gamma_o > 0$) than when the increment $d\gamma''$ is in the opposite direction ($d\gamma''/\gamma_o < 0$). The two stiffnesses are labeled $B_2^{\text{ep},+}$ and $B_2^{\text{ep},-}$. At the center of a developing shear band, the ratio $d\gamma''/\gamma_o$ is negative (for example, between the points b and d in Fig. 8); whereas $d\gamma''/\gamma_o$ is positive within the outer portions of a shear band (within the ranges a–b and d–e, Fig. 8). These results indicate that the strengthening effect of $d\gamma''$ will be smaller at the center of a shear band

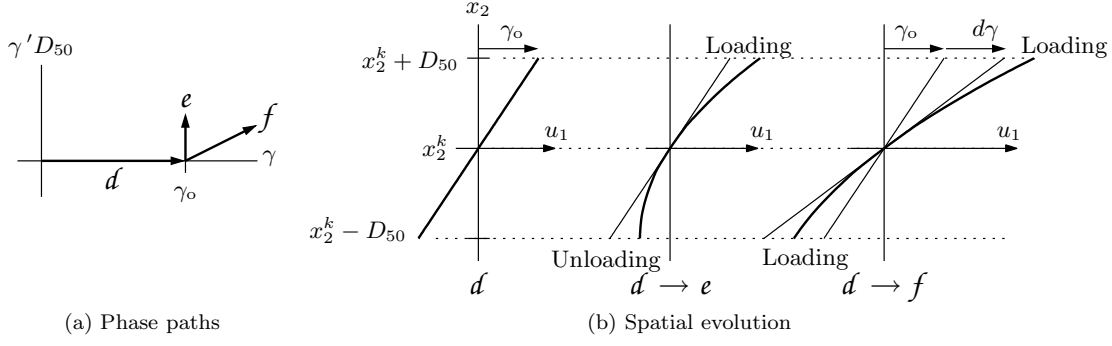


Fig. 19. A rationale for the possible coupling of $d\gamma$ and $|d\gamma'|$ in a constitutive form.

than will its weakening effect near the extremities of the shear band.

The incremental stiffness B_1^{ep} that is associated with the first gradient $|d\gamma'|$ is negative, which is consistent with the cumulative weakening effect that was observed during the Series III tests (Section 4.2). The values of B_1 in Table 2 are averages of values that were measured after first uniformly deforming the material to seven different shear strains γ_o between 0.5% and 5%. The influence of $|d\gamma'|$ at these strains, altogether absent at strain $\gamma_o = 0$, suggests that the material's initial central symmetry was broken during the earliest stage of uniform loading. This loss of symmetry should not be due to any stress-induced anisotropy of fabric that would have been produced during the initial stage of uniform shearing, since a spatially uniform deformation would have produced spatially uniform changes in fabric. The loss of central symmetry is probably due to non-linearities in the contact mechanism that would develop during any inelastic deformation (Section 4.3). Figure 19 presents a rationale for this early loss of central symmetry. The sequence $d \rightarrow e$ is a uniform deformation “ d ” to a strain $\gamma_o > 0$, followed by an increment “ e ” of purely non-uniform deformation. In stage e , the increment $|d\gamma'|$ would produce further loading, perhaps further sliding at $x_2^k + D_{50}$, but would likely produce *unloading* in the vicinity of $x_2^k - D_{50}$. This asymmetry would alter the resulting stress increment.

By extending this simple reasoning, we would expect the stress response to depend upon a coupling of the increments $d\gamma$ and $|d\gamma'|$, perhaps with a coefficient B_1^{ep} in (11) that depends upon the two increments $d\gamma$ and $|d\gamma'|$. For example, if the deformation was *nearly* uniform, with a substantial increment $d\gamma$ and a much smaller increment $|d\gamma'|$, loading and sliding would likely continue at both of the locations $x_2^k + D_{50}$ and $x_2^k - D_{50}$ (see path $d \rightarrow f$, Fig. 19). Under these conditions, any asymmetry produced by the sequence $d \rightarrow f$ would probably be less than that produced by path $d \rightarrow e$, with the latter producing a greater contribution from the term $B_1^{\text{ep}}|d\gamma'|$ in (11).

This reasoning was examined with two sets of tests in which the increments $d\gamma$ and $|d\gamma'|$ were non-zero, and in which $d\gamma''$ was zero (Section 5.2 and Conditions 4 and 5 in Table 1). Stresses were measured at locations where the ratio $|d\gamma' D_{50}|/d\gamma$ was either -0.4 or 0.4 . For both conditions, the negative value of B_1^{ep} was smaller than its value with $d\gamma = 0$, a trend that is consistent with the reasoning in the preceding paragraph. The results are summarized in Fig. 20, which includes a certain speculation: that the incremental effect of the first strain gradient $|d\gamma'|$ is entirely negated at small ratios of

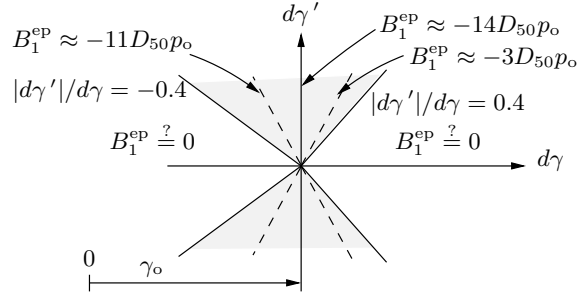


Fig. 20. Experimental values of B_1^{ep} for different combinations of $d\gamma$ and $|d\gamma'|$ in Series IV tests.

$|d\gamma'|/d\gamma$.

6 Relationship of strain gradients and localization patterns

We now explore relationships between localization patterns (Section 3) and the measured gradient-dependent behavior (Sections 4 and 5). To investigate these relationships, we construct a simple one-dimensional gradient-dependent model that is consistent with results of the constrained sinusoid tests. We then compare the behavior of the model to the localization patterns that were observed in the unconstrained shear tests. We consider both microband and shear band localizations.

6.1 Microbands and strain gradients

The experimental results in Section 5.1 show that, at very small strains, shear stress depends upon both the shearing strain γ and its second gradient γ'' . We will see that this measured behavior is consistent with the observed periodicity in microband patterning. In the absence of body forces, a simple, one-dimensional model of shearing can be constructed from the equilibrium and kinematic conditions,

$$d\bar{\sigma}_{21}/dx_2 = 0, \quad du_1/dx_2 = \gamma, \quad (12)$$

where $\bar{\sigma}_{21}$ is the shear stress at vertical position x_2 , and u_1 is the corresponding horizontal displacement. The measured small-strain material behavior in (10) can be linearized as

$$\bar{\sigma}_{21} \approx G_o\gamma + B_2\gamma'' . \quad (13)$$

Substituting (13) and (12) into (12) leads to a harmonic fourth order ordinary differential equation in the shearing displacement u_1 ,

$$B_2 u_1^{\text{iv}} + G_o u_1'' = 0, \quad (14)$$

where differentiation is with respect to the vertical position x_2 . Although an affine solution $u_1 = a + bx_2$ may apply to an ideal, homogeneous material undergoing uniform shearing, local perturbations due to material inhomogeneity will likely produce periodic solutions having the spatial periodicity $\lambda = 2\pi\sqrt{B_2/G_o}$. Experimental values of the stiffnesses B_2 and G_o were measured at the start of the Series III sinusoid shear tests, and these values suggest a periodicity in the range of $3.3D_{50}$ to $4.2D_{50}$ (see Fig. 17). This range overlaps

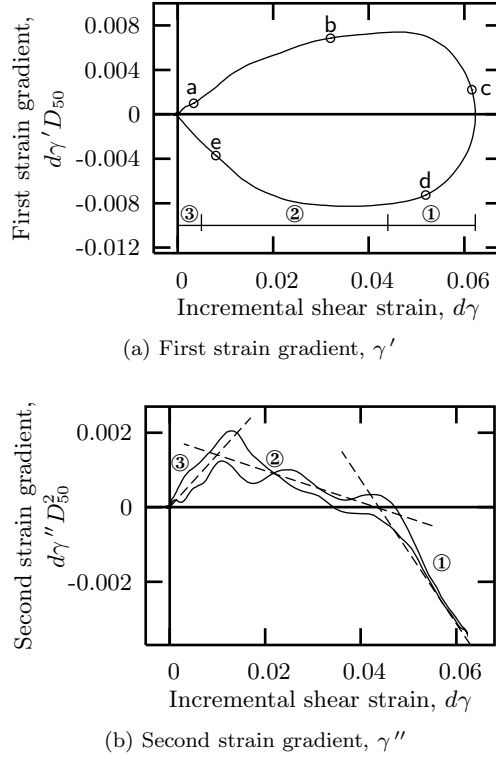


Fig. 21. The phase trajectory in $\gamma - \gamma' - \gamma''$ space for the shear band C in Fig. 8, during the strain interval of 2.0–2.5%.

the observed range of periodicities of $3.5D_{50}$ to $8D_{50}$ for the microband patterning that emerged at the very start of unconstrained shearing (Section 3.1.1 and Fig. 7). These results suggest that a gradient-dependent continuum model may account for certain features of micro-level localization.

6.2 Shear bands and strain gradient dependence

We now consider whether the observed features of shear bands are consistent with the measured effects of strain gradients. We will be primarily interested in the incremental effects of the shear strain γ and its first two derivatives, γ' and γ'' , as reported in Section 5.2. We will relate these results to the shear band observations of Section 3.1.2 by employing two separate approaches:

- We first consider internal shear band features: specifically, we investigate the strains and strain gradients within a shear band and determine whether these measurements are consistent with the separately measured incremental effects of $d\gamma$, $|d\gamma'|$, and $d\gamma''$ (Section 6.2.1).
- We also construct a simple one-dimensional model that is consistent with the measured incremental effects of $d\gamma$, $|d\gamma'|$, and $d\gamma''$, and then we test whether this model can reproduce the observed features of a shear band (Section 6.2.2).

6.2.1 Gradient-dependence within a shear band

Figure 21 shows the phase trajectory for the persistent shear band C (Section 3.1.2 and Fig. 8). Because the horizontal shear stress is uniform along the height of the assembly,

Fig. 21 gives combinations of the increments $d\gamma$, $|d\gamma'|$, and $d\gamma''$ that produce the same increment of shearing stress. The deformations were measured between the average strains $\bar{\gamma}$ of 2% and 2.5%, after band C had become persistent. Although the average strain increased by $d\bar{\gamma} = 0.5\%$, the strains are substantially larger within the shear band, where they have attained increments as large as 6%. Within the 2.0–2.5% strain interval, the material began to soften, and the shearing stress decreased by $-0.053p_o$ (see Fig. 10).

The phase plot of $d\gamma$ and $d\gamma''$ appears to hold three regions with differing behaviors (Fig. 21b). These regions are denoted with dashed trend lines and are labeled ①, ②, and ③. Behavior ① occurs near the center of the shear band (near point c in Fig. 8), where shearing strains are large and the second strain gradient $d\gamma''$ is negative. Behavior ② occurs nearer the outer portions of the band, where strains are smaller and the second gradient $d\gamma''$ is positive. The data shows a distinct change in slope for behaviors ① and ② (Fig. 21b). This change in slope is consistent with the incremental nonlinearity associated with $d\gamma''$, as was measured in the Series IV tests of Section 5.2. Indeed, if we ignore the effect of the first strain gradient $|d\gamma'|$ in (11), the line ① can be used to estimate the two moduli $G^{\text{ep},+}$ and $B_2^{\text{ep},-}$ that are associated with a positive, loading increment $d\gamma$ and a negative increment $d\gamma''$ ($d\gamma/\gamma_o > 0$, $d\gamma''/\gamma_o < 0$). The stress increment $d\bar{\sigma}_{21}$ was $-0.053p_o$, which leads to the following values of $G^{\text{ep},+}$ and $B_2^{\text{ep},-}$:

$$G^{\text{ep},+} \approx -1.2p_o, \quad B_2^{\text{ep},-} \approx -6D_{50}^2p_o. \quad (15)$$

The value of $G^{\text{ep},+}$ within the shear band is quite close to the loading modulus of $-1.0p_o$ that was measured at strains greater than 4% (Fig. 18b). The computed sign of the modulus $B_2^{\text{ep},-}$ is negative, which is also consistent with that measured in the incremental Series IV tests of Section 5.2, but the value $-6D_{50}^2p_o$ is only about half that measured in the Series IV tests ($B_2^{\text{ep},-}$ in Table 2). This difference may be the result of a possible coupling of the increments $d\gamma$ and $d\gamma''$ in their influence on the stress increment $d\bar{\sigma}_{21}$. The modulus $B_2^{\text{ep},+}$ associated with slope ② is about $-30D_{50}^2p_o$, which also differs from the value measured in Series IV tests (Table 2).

6.2.2 One-dimensional model of shear bands

We now investigate shear bands by constructing a simple one-dimensional gradient-dependent model that is consistent with the experimental results of the Series IV sinusoid tests of Section 5.2. The incremental constitutive form (11) that was constructed from the experimental results is a non-homogeneous and non-linear second order differential equation in the incremental shearing strain $d\gamma$. It is repeated here:

$$d\bar{\sigma}_{21} = G^{\text{ep}}d\gamma + B_1^{\text{ep}}|d\gamma'| + B_2^{\text{ep}}d\gamma''. \quad (11)$$

In the absence of body forces, the horizontal shearing stress $d\bar{\sigma}_{21}$ must, of course, be independent of position x_2 , as in (12₁), so $d\bar{\sigma}_{21}$ will be treated as an unknown parameter that requires solving. Equation (11) contains many complexities: incremental non-linearities that are associated with the two coefficients G^{ep} and B_2^{ep} ; a derivative $d\gamma'$ that appears in an incrementally non-linear form; and a coefficient B_1^{ep} that is a non-linear function of the ratio $|d\gamma'|/d\gamma$ (Section 5.2). Our purpose is to test whether (11) can lead to incremental solutions $du_1(x_2)$ that approximate observed shear band profiles. To this end, we note that the horizontal shearing displacement du_1 is linked to (11) by the kinematic condition (12₂). We consider boundary conditions that would apply to the upper half of

a horizontal band centered at $x_2 = 0$ within a domain $x_2 \in [-L, L]$:

$$\begin{aligned} du_1(L) &= \overline{d\gamma}L = \overline{du_1}, & du_1(0) &= 0 \\ d\gamma'(0) &= 0, & d\gamma'(L) &= 0. \end{aligned} \quad (16)$$

If the stress increment $d\overline{\sigma}_{21}(x_2)$ is constant, symmetries in (11), (12), (16) and the constitutive forms of G^{ep} , B_1^{ep} , and B_2^{ep} will impose the following symmetry condition: $d\gamma(-x_2) = d\gamma(x_2)$. The height $L = 67D_{50}$ will be half the height of the particle assembly in Fig. 1, and condition (16₄) is consistent with periodic boundaries at $-L$ and L . The displacement $\overline{du_1}$ in (16₁) will be half of the shearing displacement that occurs across the full height $[-L, L]$ between the two strains γ_o and $\gamma_o + \overline{d\gamma}$. The values of $G^{\text{ep},-}$, $B_2^{\text{ep},+}$, and $B_2^{\text{ep},-}$ are the experimental values in Fig. 18 and Table 2. The value of modulus B_1^{ep} was found to depend upon the increments $d\gamma$ and $|d\gamma'|$, and although the full nature of this relation could not be fully explored, we used a form of B_1^{ep} that was consistent with the data in Table 2 and Fig. 20.

The system of equations (11), (12), and (16) admit the trivial solution

$$du_1(x_2) = (x_2/L)\overline{du_1}, \quad (17)$$

but the non-linear system may also have other solutions as well. We used the Matlab package with its Newton–Raphson iteration scheme to seek other solutions.

The system (11), (12), and (16) also requires a choice of the loading modulus $G^{\text{ep},+}$. The Series II experiments indicated that, when deformation is constrained, the loading modulus is positive until the strain γ reaches 2.7% (Fig. 18). In unconstrained tests, non-persistent bands began to form at a shearing strain of only 0.5%, and a persistent band was active at a strain of about 2%. We were unable, however, to find a stable band-like solution to the boundary value problem when the loading modulus was uniformly positive throughout the region $[-L, L]$. This result suggests two conditions that could at first initiate and then later strengthen a shear band:

- Local softening could initiate a shear band. The evidence of Section 4.6 shows that local softening is a pervasive characteristic of granular materials (Fig. 16). The results also show that after continued deformation, regions of local weakening can later harden and heal, freezing the shear band.
- Once initiated, a shear band could become persistent if the local weakening is sustained by progressively larger strains that would produce an irrecoverable softening of the material.

The first possibility was investigated by assigning a positive value of $3p_o$ to the loading modulus $G^{\text{ep},+}$ throughout the region $[0, L]$ except within a thin weak zone near the center of a possible band, where we assign the slightly negative stiffness of $G^{\text{ep},+} = -1p_o$ (Fig. 22a). The positive value of $3p_o$ is the loading modulus that was measured in the constrained Series II tests at the strain $\overline{\gamma} = 1.6\%$ (Fig. 18a).

A stable solution of the boundary value problem is shown in Fig. 22a for the conditions that were present at the appearance of the non-persistent band B, and this solution is roughly consistent with the measured shearing profile of band B. These results show that a shear band can form in a region of local weakness while the rest of the material is undergoing a general hardening, although the band may not be persistent.

A second choice of the modulus $G^{\text{ep},+}$ was used for investigating whether the same model can predict the development of a persistent shear band. We now consider the strain

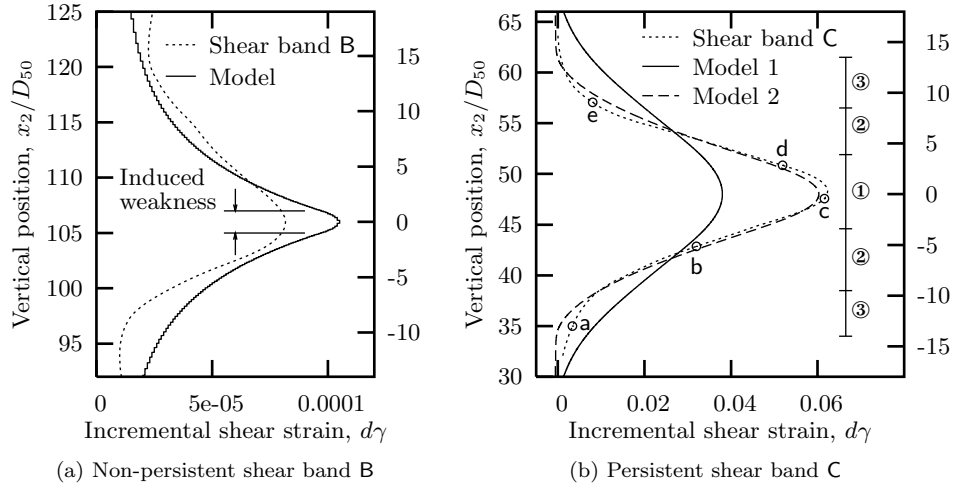


Fig. 22. Two one-dimensional models of a granular material. (a) Initiation of a non-persistent shear band. The resulting strain profile is compared with the non-persistent shear band B of Fig. 8. (b) Intensification of a persistent shear band between strains $\bar{\gamma} = 2\% - 2.5\%$. The resulting strain profiles are compared with the shear band C of Fig. 8.

interval of $\bar{d\gamma} = 2.0 - 2.5\%$, which includes both hardening and softening behaviors. Shear band C had formed and had become persistent within this strain interval, and the same range was considered in the previous Section 6.2.1 and in Figs. 9 and 21. The measured loading modulus $G^{\text{ep},+}$ is shown in Fig. 18b for strains greater than 2%, and these results suggest that a general softening occurs at strains of 2.7% and beyond. The dashed line in the figure gives the moduli $G^{\text{ep},+}$ that are used in the current model.

Two solutions to the model are shown in Fig. 22b. The solutions are compared with the strain profile that was measured within the persistent shear band C (Figs. 8, 9, and 21). One solution uses the values of moduli $B_2^{\text{ep},+}$ and $B_2^{\text{ep},-}$ given in Table 2. These “Model 1” values were independently measured in the incremental sinusoid Series IV tests, but they produce a shear band that is somewhat thicker than shear band C. A second pair of moduli were inferred in Section 6.2.1 from the measurements of $d\gamma$ and $d\gamma''$ within band C itself, and, not surprisingly, these values produce a strain profile that more closely matches band C (Model 2: $B_2^{\text{ep},+} = -30D_{50}^2p_o$, $B_2^{\text{ep},-} = -6D_{50}^2p_o$).

The regions ①, ②, and ③ in Fig. 22b correspond to those that were discussed in Section 6.2.1 (see Fig. 21). The material is softening within regions ① and ②, hardening within region ③, and unloading outside of the band. The simple model demonstrates that a shear band can become persistent when strains within the band are large enough to bring the material into a state of sustained softening, even while material near the edges and outside of the band is still hardening or is unloading.

7 Conclusions

In the preceding sections we have used simulation experiments to explore the complex behavior of granular materials. The experiments demonstrate several characteristics of these materials.

- (1) Strain localization is not an isolated phenomenon that only accompanies failure. At

each stage of unconstrained loading, deformation is concentrated within small regions. Indeed, rather aggressive means are required to suppress this tendency toward localization. At low strains, intense shearing occurs within an evolving network of microbands. At moderate strains, the deformation is concentrated within much thicker non-persistent shear bands. At yet larger strains, shear bands become stationary and persistent.

- (2) Granular materials are highly heterogeneous. Local weakening, healing, and strengthening are neither infrequent nor isolated occurrences, but are pervasive characteristics of granular discontinua.
- (3) Microbands and shear bands likely originate within weaker regions, but these regions can later strengthen, perhaps arresting one localization band while other bands are forming elsewhere.
- (4) Granular materials are non-simple. Shearing stress depends upon both the first and second gradients of shear strain.
- (5) The incremental influences of the shearing strain and its first two gradients are all non-linear and are likely coupled.
- (6) The influence of the first strain gradient suggests a lack of central symmetry in the averaged local behavior.
- (7) In spite of large fluctuations in particle rotations, they conform, on average, with the mean-field rotation, even in the presence of non-uniform deformations.
- (8) The average dilation that accompanies shearing is a function of the local strain but is independent of the gradients of strain.
- (9) An experimentally based one-dimensional continuum model can capture certain features of localization patterns. A simple second-gradient linear model can predict the spacing of microbands at small strains.
- (10) A more complex non-linear model can predict the deformation profile of a non-persistent shear band. The model requires, however, the presence of localized softening in the midst of general hardening.
- (11) An even more complex model can produce the deformation profile of a persistent shear band, within which large shearing strains produce a localized and unrecoverable softening.

In short, the experiments show that granular materials are gradient-dependent, that this dependence is measurable, and that the measurements can be applied to explain characteristics of three different localization phenomena. The experiments also reveal that the gradient-dependent behavior is quite complex, with many observed features and nonlinearities that have not yet been embodied in any current continuum, constitutive proposal. The particle simulations could, of course, be expanded to more general conditions, for example, by using three-dimensional simulations of non-spherical particles. Furthermore, the experiments have only probed the effect of the one-dimensional gradients $u_{1,2}$, $u_{1,22}$, $u_{1,222}$, etc., and other gradients would need to be explored before volumetric localization phenomena, such as compaction bands, could be modeled. These and other important effects are left for future study.

References

- Bagi K., 1999. Microstructural stress tensor of granular assemblies with volume forces. *J. Appl. Mech.* 66 (4), 934–936.
- Bazant Z.P., Belytchko T.B., Chang T.P., 1984. Continuum theory for strain-

- softening. *J. Engrg. Mech.* 110 (12), 1666–1692.
- Calvetti F., Combe G., Lanier J., 1997. Experimental micromechanical analysis of a 2D granular material: relation between structure evolution and loading path. *Mech. of Cohesive-Frictional Mat.* 2 (2), 121–163.
- Chang C.S., Gao J., 1995. Second-gradient constitutive theory for granular material with random packing structure. *Int. J. Solids and Structures* 32 (16), 2279–2293.
- Cundall P.A., Strack O.D.L., 1979. A discrete numerical model for granular assemblies. *Géotechnique* 29 (1), 47–65.
- Finno R.J., Alarcon M.A., Mooney M.A., Viggiani G., 1997. Shear bands in plane strain active tests of moist tamped and pluviated sands. In: of XIV ICSMFE P.C. (ed.), *Proc. of the Fourteenth Intern. Conf. on Soil Mech. and Foundation Engrg.*, A.A. Balkema, Rotterdam, vol. 1, pp. 295–298.
- Fleck N.A., Hutchinson J.W., 1997. Strain gradient plasticity. In: Hutchinson J.W., Wu T.Y. (eds.), *Advances in Applied Mechanics*, Academic Press, San Diego, Ca., vol. 33, pp. 295–361.
- Iwashita K., Oda M., 1998. Rolling resistance at contacts in simulation of shear band development by DEM. *J. Engrg. Mech.* 124 (3), 285–292.
- Koenders M.A., 1990. Localized deformation using higher order stress/strain theory. *J. Energy Res. Tech.* 112 (1), 51–53.
- Kuhn M.R., 1999. Structured deformation in granular materials. *Mech. of Materials* 31 (6), 407–429.
- Kuhn M.R., 2003. An experimental method for determining the effects of strain gradients in a granular material. *Comm. Numer. Methods Engrg.* p. In printing.
- Mühlhaus H.B., Oka F., 1994. A gradient elasticity model for granular materials. In: Chambon R., Desrues J., Vardoulakis I. (eds.), *Localisation and Bifurcation Theory for Soils and Rocks*, A. A. Balkema, Rotterdam, The Netherlands, pp. 201–209.
- Noll W., 1958. A mathematical theory of the mechanical behavior of continuous media. *Arch. Rational Mech. Anal.* 2 (3), 197–226.
- Oda M., Konishi J., Nemat-Nasser S., 1980. Some experimentally based fundamental results on the mechanical behaviour of granular materials. *Géotechnique* 30 (4), 479–495.
- Vardoulakis I., 1998. Strain localization in granular materials. In: Cambou B. (ed.), *Behaviour of Granular Materials*, Springer, Vienna, pp. 339–400.
- Vardoulakis I., Aifantis D.C., 1991. A gradient flow theory of plasticity for granular materials. *Acta Mechanica* 87 (3), 197–217.
- Vermeer P.A., Brinkgreve R.B.J., 1994. A new effective non-local strain-measure for softening plasticity. In: Chambon R., Desrues J., Vardoulakis I. (eds.), *Localisation and Bifurcation Theory for Soils and Rocks*, A. A. Balkema, Rotterdam, pp. 89–100.